Chinese Chemical Letters 34 (2023) 107797

Contents lists available at ScienceDirect

Chinese Chemical Letters

journal homepage: www.elsevier.com/locate/cclet

Advancing knowledge of plasma spraying coatings for Li||Sb-Sn liquid metal batteries by X-ray micro-CT

Kaixuan Cui[a,b], Ping Li[a,*], Wang Zhao[c], Chunrong Liu[a], Qi Wan[d,e], Shengwei Li[a], Xuanhui Qu[a]

[a] Beijing Advanced Innovation Center for Materials Genome Engineering, Institute for Advanced Materials and Technology, University of Science and Technology Beijing, Beijing 100083, China
[b] Beijing Key Laboratory of Membrane Materials and Engineering, Department of Chemical Engineering, Tsinghua University, Beijing 100084, China
[c] Institute of Science and Technology, China Three Gorges Corporation, Beijing 100038, China
[d] School of Materials Science and Engineering, Southwest University of Science and Technology, Mianyang 621010, China
[e] Shanxi Beike Qiantong Energy Storage Science and Technology Research Institute Co., Ltd., Gaoping 048400, China

ARTICLE INFO

Article history:
Received 27 July 2022
Revised 17 August 2022
Accepted 1 September 2022
Available online 5 September 2022

Keywords:
Liquid metal batteries
Sb-Sn corrosion
Plasma-sprayed W coating
SS304 matrix
Micro-CT nondestructive inspection

ABSTRACT

The performance of Li||Sb-Sn liquid metal batteries (LMBs) is hindered by the corrosion of the Sb-Sn cathode on its current collector. Herein, a uniform, dense, and low-oxidized W coating was prepared by plasma spraying, which can effectively resist the corrosion of the cathode and improve the cycle stability of the Li||Sb-Sn LMBs. For the first time, micro-CT nondestructive inspection is applied in the field of LMBs. The corrosion micromorphology and composition evolution of the SS304 matrix and Sb-Sn cathode with or without the plasma-sprayed W coating is obtained without disassembling the battery, which proves that the W coating can effectively protect the SS304 matrix. Our autonomous new LMB device for nondestructive inspection is universal and can be applied to different LMBs systems for advancing knowledge of corrosion mechanism and protection. This work guarantees the ability to directly visualize the inner critical positions in three dimensions and fills the knowledge gap in the field of LMB detection technology.

Liquid metal batteries (LMBs) are among the emerging sustainable battery technologies for the renewable energy revolution [1–6]. Among them, Li||Sb-Sn LMBs have exhibited distinguished cycle performance, excellent rate capability, and unprecedented thermal robustness [4]. However, the liquid Sb-Sn cathode severely corrodes with the commonly used stable cathode current collectors, such as stainless steels, Ti, and Mo [7,8]. Fortunately, W has been proven to be an admirably stable cathode current collector of Li||Sb-Sn LMBs [8], and it is considered to act as a protective coating material to reduce cost and solve the difficult-to-form problem.

To date, plasma spraying surface engineering technology has played an important role in the field of corrosion and protection [9–12], where the solid spraying material is heated to a molten or semi-molten state by a spray gun, sprayed on the surface of the treated workpiece, and deposited to form a coating with a certain thickness. Compared with other deposition technologies, plasma spraying is simple in operation and has favorable cost effectiveness. It can quickly prepare coatings with different thicknesses, and it is not limited by the shape of the matrix material. In addition, stainless steels are first qualified for the matrix material because of their excellent comprehensive properties, especially their high strength and compatibility with W (similar thermal expansivity and conductivity) [13–18]. To date, there have been many studies on the preparation of W coatings by plasma spraying, but no relevant reports are found in the field of LMBs. In brief, to fabricate a cathode protective coating in Li||Sb-Sn LMBs to enhance their performance, some in-depth, sufficient and comprehensive analytical investigations must be executed.

However, the commonly used detection and analysis methods such as X-ray diffraction (XRD), scanning electron microscopy (SEM), and X-ray photoelectron spectroscopy (XPS), must disassemble the batteries, destroy their structure (especially thin coating), and affect their service life, but they cannot completely and explicitly demonstrate the structure and morphology of the detected position. X-ray micro computed tomography (micro-CT), a nondestructive inspection technology that produces high-resolution (micron to submicron) image stacks to generate digital three-dimensional models of samples opportunely solve

* Corresponding author.
E-mail address: ustbliping@126.com (P. Li).

https://doi.org/10.1016/j.cclet.2022.107797
1001-8417/

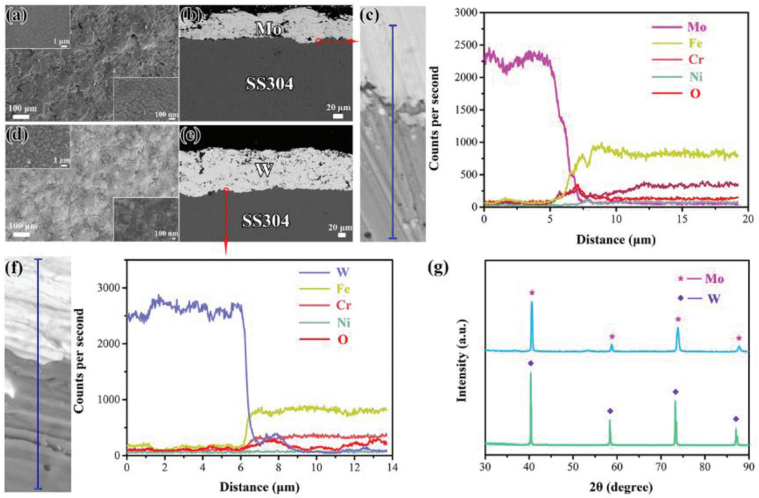

Fig. 1. (a) SEM images of the prepared Mo coating surface. (b) Cross-sectional SEM image at the junction of the prepared Mo coating and SS304 matrix. (c) EDS line analysis at the junction of the prepared Mo coating and SS304 matrix. (d) SEM images of the prepared W coating surface. (e) Cross-sectional SEM image at the junction of the prepared W coating and SS304 matrix. (f) EDS line analysis at the junction of the prepared W coating and SS304 matrix. (g) XRD patterns of the prepared Mo and W coating.

these above problems. X-ray micro-CT has opened up a new field of application in batteries, *e.g.*, lithium-ion batteries, fuel cells, and solid-state batteries [19–22]. However, the potential of X-ray micro-CT for probing LMBs, especially the morphology observations of the electrodes and electrolytes, has not been developed due to their sophisticated and thick shell for sealing.

Herein, nondestructive micro-CT, which also guarantees the ability to directly three-dimensionally visualize the inner critical positions, is employed to preliminarily fill the knowledge gap in the field of LMB detection technology. Specifically, a new LMB device for nondestructive micro-CT was designed and fabricated, which can serve as a cell for electrochemical testing and for high-resolution nondestructive micro-CT inspection. The resolution of micro-CT is now up to the micron or even nanometer scale, and this device can adjust its material and size to meet the resolution requirements. So it is theoretically feasible to infer the corrosion mechanism by observing the corrosion morphology and composition evolution of key parts of different LMBs systems by micro-CT. In this work, we focus on observing the state changes of corrosion interfaces between the coating and the matrix after cell cycling and proves that the W coating can effectively protect the SS304 matrix from the corrosion of the Sb-Sn cathode.

The SEM-EDS images of the coatings prepared by plasma spraying are shown in Fig. 1. The Mo coating has excellent crystallinity: the dense and uniform grains are closely arranged and stacked in a lamellar shape with a thickness of ~50 μm (Figs. 1a and b). The EDS line analysis at the junction of the Mo coating and SS304 matrix (Fig. 1c) can intuitively reveal the content of each element in the area of the line segment, apparently, the O content in the Mo coating is fairly low, which will hardly lower the conductivity. Notably, there is a composition transition region between the Mo coating and the SS304 matrix (Fe/Cr), which indicates that metallurgical reactions may have occurred at the moment when the high-temperature molten Mo was sprayed onto SS304; *i.e.*, the atoms at the interface of Mo and SS304 diffused and alloyed with each other (to form Fe-Mo and Cr-Mo products) [23–25].

In addition, the W coating has excellent crystallinity: Dense and uniform grains are closely arranged and stacked in a lamellar shape with a thickness of ~100 μm (Figs. 1d and e). The EDS line analysis at the junction of the W coating and SS304 matrix (Fig. 1f) can intuitively reveal that the O content in the W coating is fairly low and it will hardly lower its conductivity. Unlike the Mo coating, there is no obvious composition transition region between the W coating and SS304 (Fe/Cr), but the W content suddenly drops at the interface, which suggests that the main combination form is mechanical bonding. In other words, the W particles collide on the matrix into a flat shape and fit with the uneven surface to form a stable bond (anchor effect) by mechanical interlocking among particles.

Mo and W coatings combine with SS304 in different modes because molten W is difficult to dissolve in Fe and Cr to form alloys, while Mo tends to dissolve in Fe and Cr to form alloys even at a high temperature above 10,000 °C. The XRD patterns of the Mo and W coating surfaces (Fig. 1g) clearly show no obvious impurity phases except for Mo and W, whose peak shapes are sharp and symmetrical, which exhibit excellent crystallinity, and are consistent with the above SEM-EDS analysis.

Next, static corrosion (500 °C, 500 h) between Mo/W coating and Sb-Sn alloy was performed to analyze their corrosion resistance to the Sb-Sn alloy at the operating temperature of LMBs. Fig. S1 (Supporting information) displays the SEM-EDS mappings of the corrosion interface between Mo/W coating and Sb-Sn alloy after static corrosion. Apparently, hardly any Mo coating can be found in the interface range in Fig. S1a; some Fe has been precipitated from the SS304 matrix, dissolved in the Sb-Sn alloy, and combined with the active element Sb. However, the W coating was largely preserved with an uneven surface after static corrosion (Fig. S1b), which demonstrates that the W coating was also corroded and fell off, but the SS304 matrix was unaffected and intact. Although metallurgical bonding has a stronger binding force than mechanical bonding [26–28], Mo is easily dissolved in Sb-Sn, which makes the Mo coating disappear. Fortunately, W is almost insoluble in Sb-Sn and can resist dissolution corrosion, but some fragments of the W coating will inevitably fall off due to cavitation corrosion [8].

Li||Sb-Sn LMBs were prepared with Mo and W coatings (SS304 matrix) as cathode current collectors respectively to explore their practical service characteristics. Figs. 2a and b show the electrochemical performance of a Li||Sb-Sn LMB with a Mo coating as the cathode current collector, where Fig. 2a shows the voltage-capacity profiles of the 1st, 5th, 10th and 15th charge-discharge cycles, and Fig. 2b shows the variation in capacity and Coulombic efficiency with the cycle number. Specifically, in the initial stage of cell cycling, the cell voltage and capacity are stable with no abnormalities. Then, the overpotential increases, and a new low plateau ap-

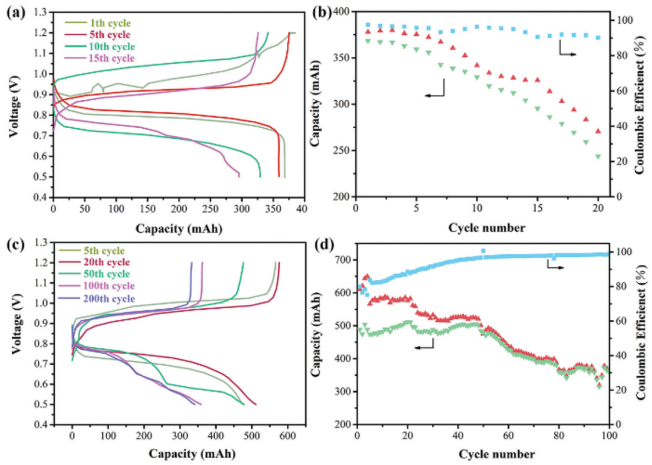

Fig. 2. Electrochemical performance of Li||Sb-Sn LMBs with Mo coating as a positive current collector: (a) Profiles of voltage and capacity during charge and discharge (the 1st, 5th, 10th and 15th cycle). (b) Charge capacity, discharge capacity, and Coulombic efficiency as a function of cycle number. Electrochemical performance of Li||Sb-Sn LMBs with W coating as a positive current collector: (c) Profiles of voltage and capacity during charge and discharge (the 5th, 20th, 50th, 100th and 200th cycle); (d) Charge capacity, discharge capacity and Coulombic efficiency as a function of cycle number.

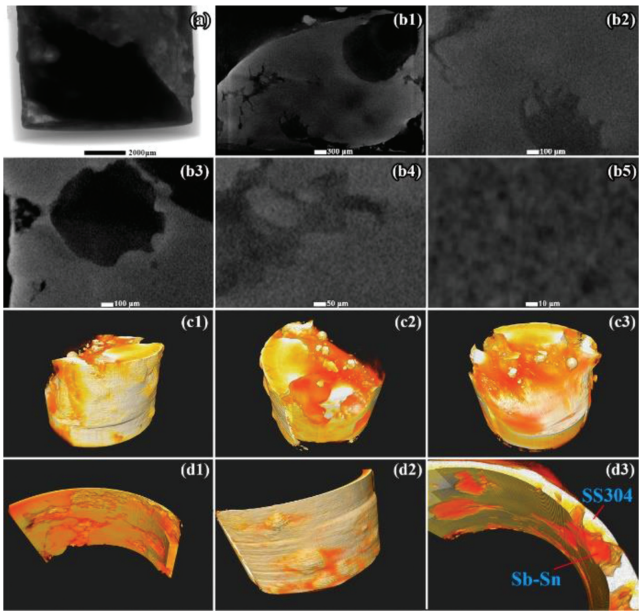

Fig. 3. (a) Digital radiography of the SS304 and Sb-Sn alloy after static corrosion. (b) Two-dimensional CT tomography images of the SS304 and Sb-Sn alloy after static corrosion. (c) Three-dimensional reconstructed images of Sb-Sn alloy. (d) Three-dimensional reconstructed images of the corrosion interface between SS304 and Sb-Sn alloy. The operating temperature and time of static corrosion condition is 500 °C and 168 h, respectively.

pears in the discharge voltage-capacity profile, with a Coulombic efficiency over 90%. Based on static corrosion results, it can be determined that the Mo coating corrodes with the cathode (forming Mo-Sb-Sn corrosion products [8]) and subsequently falls off. Therefore, SS304 directly contacts and corrodes with the cathode and forms Fe-Ni-Sb-Sn corrosion products, which can participate in lithiation and decrease the cell discharge voltage and capacity [7].

Furthermore, Figs. 2c and d show the electrochemical performance of a Li||Sb-Sn LMB with a W coating as the cathode current collector, where Fig. 2c shows the voltage-capacity profiles of the 5th, 20th, 50th, 100th and 200th charge-discharge cycles, and Fig. 2d shows the variation of the capacity and Coulombic efficiency with cycle number. The cell voltage and capacity are stable, while the Coulombic efficiency steadily increases in the first dozens of charge-discharge cycles. However, a new low plateau appears in the discharge voltage-capacity profile, the cell capacity rapidly decays at the 50th charge-discharge cycle, the capacity restores stability after the 80th cycle, and the Coulombic efficiency reaches 99%. Based on static corrosion results, the W coating can effectively resist the corrosion of the cathode (the charging state is Sb-Sn, and the discharging state is Li-Sb, Sb-Sn and Sn) during the first 50 cycles, after which the W coating gradually falls off due to corrosion (erosion and cavitation corrosion) [8]. Consequently, SS304 directly contacts the cathode, and a large amount of Fe and Ni in SS304 will dissolve in the cathode, which severely deteriorates the cell performance [7]. The dissolution tends to be saturated after the 80th cycle, and the voltage and capacity of the cell gradually stabilize.

After the above two cells completed the charge-discharge cycle and cooled to room temperature, XRD phase analysis was performed on their cathode mixtures (Fig. S7 in Supporting information), where some Mo and W phases were found, which corresponds to the peeled coating on the surface of SS304. A certain amount of corrosion products, such as $Fe_{2.55}Sb_2$, $NiSb_2$ and $FeSn_2$, were found in both mixtures (unmarked peaks are SS304 and electrolyte, *etc.*), which verifies the above inference of the corrosion process. In summary, the W coating can effectively resist the corrosion of the cathode for a certain period of time, protect the SS304 matrix and improve the cycle stability of the Li||Sb-Sn LMBs.

In this work, a nondestructive inspecting device for LMBs was designed and fabricated, and the micromorphology of key parts of LMBs can be obtained by applying nondestructive micro-CT inspection. Fig. S8 (Supporting information) shows the overall X-ray digital radiography image of the device, the different positions (components) of which show different grayscale values due to different X-ray absorption rates. Combined with Fig. S2a (Supporting information), the cathode, anode, electrolyte, cathode current collector, anode current collector, insulating ceramic, and coating can be clearly identified. First, the digital radiography of the SS304 and Sb-Sn alloy after static corrosion (500 °C, 168 h) is shown in Fig. 3a. This figure gradually darkens from the outside to the inside, which are the titanium alloy shell, SS304 and Sb-Sn cathode. It may be caused by the cooling shrinkage, where some holes and cracks in the cathode can be found in the two-dimensional tomography images (Fig. 3b). Unfortunately, the corrosion interface between Sb-Sn and SS304 cannot be distinguished due to the close grayscale values at different positions.

As is well known, the micro-CT device can generate a series of two-dimensional tomography images at different depths of the tested sample in the process of rotating the object around a single axis. The obtained two-dimensional images can be processed (filtering and denoising, threshold segmentation, *etc.*) and stacked in a certain order to get a three-dimensional reconstruction image reflecting the internal structure of the tested sample. Here, the VoxelStudio Recon reconstruction software was used to reconstruct the two-dimensional images into three-dimensional images. Fig. 3c shows the three-dimensional images of the SS304 and Sb-Sn alloy from different angles after static corrosion (500 °C, 168 h); unfortunately, the corrosion behavior between them still could not be determined. The mutual penetration and dissolution of SS304 and Sb-Sn resulted in close densities and consequently close X-ray absorptivity, and the corrosion interface is difficult to distinguish. Therefore, the grayscale window width of the images was adjusted by the software to highlight the corrosion interface (Fig. 3d). The uneven orange-yellow color material corresponds to the

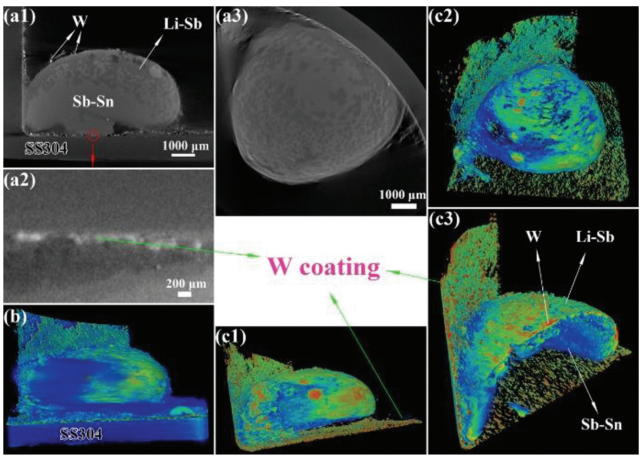

Fig. 4. (a) Two-dimensional CT tomography images of the cathode and its current collector. (b) Three-dimensional reconstructed image of the cathode and its current collector. (c) Three-dimensional reconstructed images of the corrosion interface between SS304 and Sb-Sn alloy. The operating temperature and time of static corrosion condition is 500 °C and 168 h, respectively.

Sb-Sn cathode, and the white color material corresponds to the SS304 cathode current collector with a thickness of ~1000 μm. Obviously, many concave holes have been found in SS304, some of which even run through the entire SS304 layer, and they are filled with the Sb-Sn cathode. The above analysis more intuitively indicates that serious dissolution corrosion occurred between SS304 and Sb-Sn after only 168 h of static corrosion, which is a major factor in cell performance degradation.

To highlight the corrosion resistance of the W coating prepared by plasma spraying, a Li||Sb-Sn LMB with a W coating as the cathode current collector was tested and analyzed by nondestructive micro-CT inspection after cycling (23 cycles, ~275 h). Fig. 4a shows two-dimensional tomography images of the cathode and its current collector. Unlike the above static corrosion (Fig. 3), the titanium alloy shell was replaced by SS304 based on optimizing the processing technology, and the W coating was directly sprayed on the inner surface of the SS304 shell. Therefore, the SS304 layer, W coating and droplet-shaped cathode are sequentially observed from the outside to the inside (Fig. 4a1). When the higher-density Sb reacted with the lower-density Li, a Li-Sb product was generated with a density between them. While Sn has a slightly higher density than Sb, Sb-Sn has a higher density than Li-Sb. Consequently, the grayscale of Sb-Sn in the two-dimensional tomography image obtained by micro-CT is larger than that of Li-Sb; in other words, Sb-Sn is brighter than Li-Sb. By that analogy, the higher-density W is approximately white in two-dimensional tomography images. After cell cycling, the W coating with a thickness of 100 μm is no longer uniform and dense due to erosion and cavitation corrosion, and many defects appear; correspondingly, many W fragments have been found in the cathode, but the SS304 matrix does not appear to have suffered significant corrosion. In addition, some Li_3Sb discharge products can be found in the upper part of the cathode due to incomplete charging and self-discharge when cooling.

The VoxelStudio Recon reconstruction software was implemented to reconstruct the two-dimensional tomography images of the cathode and its current collector of this Li||Sb-Sn LMB at different depths into a three-dimensional image (Fig. 4b). Sb-Sn, Li-Sb, W coating, and SS304 can be clearly identified because different grayscale positions of the image show different colors after rendering. The SS304 matrix protected by the W coating has not been significantly corroded, while SS304 without the W coating (Fig. 3) suffered serious dissolution corrosion, which indicates that the W coating has excellent service characteristics. Furthermore, the grayscale window width of Fig. 4b was adjusted, and the SS304 matrix was hidden, which highlights the contact surface between the cathode and the W coating (Fig. 4c). The bottom and side surfaces of the droplet-shaped cathode are W coatings with a thickness of ~100 μm. Apparently, the W coating in contact with the cathode (bottom surface) is sparse due to corrosion, while the W coating not in contact with the cathode (side surface) is more complete and uniform. The dissolution corrosion between SS304 and Sb-Sn has not occurred at this point, the cell performance would not be influenced, which corresponds to the first 50 cycles of the cell with W coating as the cathode current collector in Figs. 2c and d.

Since the currently prepared coating is only 100 μm thick, increasing the thickness may enhance its stability and inhibit shedding. In addition, adding a small amount of carbides to W (such as W-C) can refine the grains and strengthen the grain boundaries [29–31] to solve the easy embrittlement problem of W, reduce the erosion and cavitation between W and the cathode, and inhibit shedding. Notably, C in W-C is considered to form alloys with Fe and Cr at a high temperature [32–36], so it is likely to form a stronger metallurgical combination with the stainless-steel matrix during plasma spraying to enhance the stability of the prepared coating. It is theoretically easy to increase the coating thickness and spray the W-C coating, which we can attempt in future work to inhibit corrosion from the cathode and improve the cycle stability of Li||Sb-Sn LMBs.

In summary, a new LMB device was designed and fabricated in this work, which can perform electrochemical tests as an LMB, and perform nondestructive inspection without disassembling the battery and destroying its key parts. The corrosion micromorphology of the SS304 matrix and Sb-Sn cathode with or without plasma-sprayed W coating can be observed by micro-CT without disassembling the battery, which proves that the W coating can effectively protect the SS304 matrix. Therefore, the W coating has excellent service characteristics as a cathode current collector for Li||Sb-Sn LMBs. In addition, the methods of increasing the W coating thickness and adding a small amount of carbides to W are proposed to improve the stability of the W coating, which indicates the direction to inhibit the corrosion of liquid active electrodes on their current collectors at a high temperature. Plasma spraying technology is supposed to play an increasingly important role in solving the corrosion problem of liquid electrodes on current collectors in the emerging field of LMBs, improving the cycle stability of LMBs and facilitating their commercial applications. And micro-CT is expected to be able to observe the micromorphology and composition evolution of key parts of different LMBs systems to continuously advance the knowledge of corrosion mechanism and service characteristics of coatings in future.

Declaration of competing interest

The authors declare that they have no known competing financial interests or personal relationships that could have appeared to influence the work reported in this paper.

Acknowledgment

This work was supported by the National Key R&D Program of China (No. 2018YFB0905600).

Supplementary materials

Supplementary material associated with this article can be found, in the online version, at doi:10.1016/j.cclet.2022.107797.

References

[1] D.J. Bradwell, H. Kim, A.H. Sirk, D.R. Sadoway, J. Am. Chem. Soc. 134 (2012) 1895–1897.
[2] K. Wang, K. Jiang, B. Chung, et al., Nature 514 (2014) 348–350.
[3] X.H. Ning, S. Phadke, B. Chung, et al., J. Power Sources 275 (2015) 370–376.
[4] H. Li, K. Wang, S. Cheng, K. Jiang, ACS Appl. Mater. Interfaces 8 (2016) 12830–12835.
[5] H. Li, K. Wang, H. Zhou, et al., Energy Storage Mater. 14 (2018) 267–271.
[6] K. Cui, W. Zhao, S. Li, et al., ACS Sustain. Chem. Eng. 10 (2022) 1871–1879.
[7] K. Cui, F. An, W. Zhao, et al., J. Phys. Chem. C 125 (2021) 237–245.
[8] K. Cui, W. Zhao, D. Zhou, et al., ACS Appl. Energy Mater. 4 (2021) 9013–9021.
[9] Z. Zhou, S. Guo, S. Song, W. Yao, C. Ge, Fusion Eng. Des. 86 (2011) 1625–1629.
[10] J. Huang, X. Li, J. Chen, et al., J. Nucl. Mater. 432 (2013) 16–19.
[11] T. Liu, S.W. Yao, L.S. Wang, et al., J. Therm. Spray Technol. 25 (2016) 213–221.
[12] V. Sreenivasulu, M. Manikandan, Surf. Coat. Technol. 337 (2018) 250–259.
[13] F.L. Yaggee, E.R. Gilbert, J.W. Styles, J. Less Common Met. 19 (1969) 39–51.
[14] C.S. Kim, ANL-75-55, Argonne National Laboratory, U. S. A., 1975.
[15] R. Bogaard, P. Desai, H. Li, C. Ho, Thermochim. Acta 218 (1993) 373–393.
[16] H.K. Kang, J. Nucl. Mater. 335 (2004) 1–4.
[17] Y. Lv, J. Song, Y. Lian, et al., J. Nucl. Mater. 457 (2015) 317–323.
[18] S. Heuer, J. Matějíček, M. Vilémová, et al., Surf. Coat. Technol. 366 (2019) 170–178.
[19] E. Wargo, V. Schulz, A. Çeçen, S. Kalidindi, E. Kumbur, Electrochim. Acta 87 (2013) 201–212.
[20] F. Sun, X. He, X. Jiang, et al., Mater. Today 27 (2019) 21–32.
[21] J. Tippens, J.C. Miers, A. Afshar, et al., ACS Energy Lett. 4 (2019) 1475–1483.
[22] M. Lucero, S. Qiu, Z. Feng, Carbon Energy 3 (2021) 762–783.
[23] A. Guillermet, Bull. Alloy Phase Diagrams 3 (1982) 359–367.
[24] M. Venkatraman, J. Neumann, Bull. Alloy Phase Diagrams 8 (1987) 216–220.
[25] V. Rajkumar, K.H. Kumar, J. Alloy Compd. 611 (2014) 303–312.
[26] T. Hussain, D.G. McCartney, P.H. Shipway, D. Zhang, J. Therm. Spray Technol. 18 (2009) 364–379.
[27] J.J. Tian, S.W. Yao, X.T. Luo, C.X. Li, C.J. Li, Acta Mater. 110 (2016) 19–30.
[28] L.Y. Chen, H. Wang, C. Zhao, et al., Surf. Coat. Technol. 369 (2019) 31–43.
[29] H. Kurishita, S. Matsuo, H. Arakawa, et al., J. Nucl. Mater. 398 (2010) 87–92.
[30] H. Kurishita, H. Arakawa, S. Matsuo, et al., Mater. Trans. 54 (2013) 456–465.
[31] X.Y. Tan, L.M. Luo, Z.L. Lu, et al., Powder Technol. 269 (2015) 437–442.
[32] J. Chipman, Metall. Mater. Trans. B 3 (1972) 55–64.
[33] J.O. Andersson, Metall. Trans. A 19 (1988) 627–636.
[34] S. Atamert, H. Bhadeshia, Mater. Sci. Eng. A 130 (1990) 101–111.
[35] M. Venkatraman, J.P. Neumann, Bull. Alloy Phase Diagrams 11 (1990) 152–159.
[36] A.V. Khvan, B. Hallstedt, C. Broeckmann, Calphad 46 (2014) 24–33.